A laser photofragmentation time-of-flight mass spectrometric study of acetophenone at 193 and 248 nm

H.-Q. Zhao, Y.-S. Cheung, C.-L. Liao, C.-X. Liao, C. Y. Ng, and Wai-Kee Li

---

Articles you may be interested in

A 193 nm laser photofragmentation time-of-flight mass spectrometric study of chloroiodomethane
J. Chem. Phys. **123**, 174316 (2005); 10.1063/1.2074507

Photodissociation of bromoform cation at 308, 355, and 610 nm by means of time-of-flight mass spectroscopy and ion velocity imaging
J. Chem. Phys. **118**, 3083 (2003); 10.1063/1.1537691

Photodissociation dynamics of CH 2 BrCl studied using resonance enhanced multiphoton ionization (REMPI) with time-of-flight mass spectrometry
J. Chem. Phys. **111**, 5771 (1999); 10.1063/1.479874

Ionization and dissociation mechanism of superexcited ketene using time-of-flight mass spectrometer
J. Chem. Phys. **107**, 3797 (1997); 10.1063/1.474738

A 193-nm-laser photofragmentation time-of-flight mass spectrometric study of dimethylsulfoxide
J. Chem. Phys. **106**, 86 (1997); 10.1063/1.473025

A laser photofragmentation time-of-flight mass spectrometric study of acetophenone at 193 and 248 nm

H.-Q. Zhao, Y.-S. Cheung, C.-L. Liao, C.-X. Liao, and C. Y. Ng
Ames Laboratory,[a] United States Department of Energy, and Department of Chemistry, Iowa State University, Ames, Iowa 50011

Wai-Kee Li
Department of Chemistry, The Chinese University of Hong Kong, Shatin, N.T., Hong Kong

The photodissociation of acetophenone ($C_6H_5COCH_3$) at 193 and 248 nm has been studied using the time-of-flight mass spectrometric technique. For $h\nu = 193$ nm, two major primary channels, $C_6H_5COCH_3 + h\nu \rightarrow C_6H_5CO + CH_3$ [channel (1)] and $C_6H_5 + CH_3CO$ [channel (2)], are observed with comparable cross sections. Data analysis shows that $\approx 30\% - 50\%$ of primary C_6H_5CO and CH_3CO radicals further decomposes, yielding secondary products $C_6H_5 + CO$ and $CH_3 + CO$, respectively. The translational energy release measurements indicate that for both channels (1) and (2) at 193 nm, $\approx 25\% - 30\%$ of the available energy is channeled into kinetic energies of the primary photofragments. Measurements at $h\nu = 248$ nm reveal that the branching ratio of channel (2) to channel (1) is ≈ 0.01. For channel (1) at $h\nu = 248$ nm, $\approx 42\%$ of the available energy is directed as the kinetic energy of the photofragments. The observed maximum kinetic energy release for channel (1) at 248 nm yields a value of 85.0 ± 2.2 kcal/mol for the $C_6H_5CO-CH_3$ bond dissociation energy at 0 K (D_0). The photofragment angular distributions are found to be isotropic for both channels (1) and (2) at $h\nu = 193$ nm and for channel (1) at $h\nu = 248$ nm. A minor photodissociation channel $C_6H_5COCH_3 + h\nu \rightarrow C_6H_5CH_3 + CO$ is identified at both $h\nu = 193$ and 248 nm. The energetics for the dissociation reactions of acetophenone have also been investigated using *ab initio* Gaussian-2-type procedures. The heats of formation at 0 K ($\Delta_f H°_0$) for C_6H_5CO and C_6H_5 calculated using the isodesmic reaction scheme are 33.9 ± 1.3 and 87.6 ± 1.0 kcal/mol, respectively. These results suggest that the literature $\Delta_f H°_0$ values for C_6H_5CO and C_6H_5 are likely to be low by 3–4 kcal/mol. These theoretical $\Delta_f H°$ values for C_6H_5CO and C_6H_5 yield a theoretical $D_0(C_6H_5CO-CH_3)$ value of 85.1 ± 1.4 kcal/mol, which is in excellent accord with the experimental results obtained in the present study. © *1997 American Institute of Physics.*
[S0021-9606(97)00542-4]

I. INTRODUCTION

The ultraviolet (UV) photochemistry of alkyl ketones[1–5] and related molecules[5–9] has been the subject of many recent laser excitation studies. Upon absorption of a UV photon, ketones are known to dissociate efficiently via C–CO bond cleavage, resulting in acyl and alkyl radicals.[1–5,10] Since the C–CO bond of an acyl radical is weak, excited acyl radicals formed at a sufficiently high internal energy have been found to undergo further decomposition, producing CO and alkyl radicals.[1,5,7,11] Acyl and alkyl radicals are important intermediates in combustion and atmospheric process.[12] The knowledge of the UV photochemistry of ketones is relevant for the preparation of these radicals for spectroscopic and reactivity studies. Recent excimer laser photofragmentation time-of-flight (TOF) mass spectrometric experiments have provided detailed information concerning the dissociation mechanism of acetone (CH_3COCH_3).[1,2] Both acetyl (CH_3CO) and methyl (CH_3) radicals are observed in the 248 nm photodisso-

ciation of CH_3COCH_3, whereas $CO + 2CH_3$ are identified to be products at 193 nm.[1] An analysis of the TOF spectra for CH_3 and CO has established that the formation of $CO + 2CH_3$ from CH_3COCH_3 at 193 nm is governed by a stepwise mechanism.[1]

The photochemistry of acetophenone ($C_6H_5COCH_3$), the simplest aromatic ketone, has received little attention compared to that of CH_3COCH_3. Early photochemical studies of acetophenone were motivated by the search for a convenient source of phenol radicals.[13,14] The gas phase absorption spectrum for $C_6H_5COCH_3$ in the region of 210–380 nm exhibits three broad peaks centered at 325, 275, and 230 nm, which are assigned to the $S_0 \rightarrow S_1$, $S_0 \rightarrow S_2$, and $S_0 \rightarrow S_3$ transitions, respectively.[10,15] The absorption cross section for the $S_0 \rightarrow S_3$ peak is significantly stronger than that of the $S_0 \rightarrow S_2$ peak, which is in turn stronger than that of the $S_0 \rightarrow S_1$ peak. The first excited singlet S_1 or $^1(n, \pi^*)$ state of acetophenone is formed by an electron from the nonbonding orbital (n) localized at the O atom being excited to the antibonding π^* orbital of the carbonyl group. The existence of an aromatic ring adjacent to the carbonyl group in simple aromatic ketones, such as acetophenone, is likely to facilitate intramolecular energy transfer, and hence inhibits the disso-

ciative channels. Due to a small energy gap between the S_1 and T_1 [or $^3(n, \pi^*)$] states, the S_1 states of simple aromatic ketones are known to undergo rapid intersystem crossing to the T_1 state, resulting in high phosphorescence quantum yields.[10,15] Similar intersystem crossing processes are expected to follow the S_2 and S_3 states. Thus, the photochemistry of S_1, as well as S_2 and S_3 states, may actually take place from triplet potential energy surfaces.

The present work deals with the measurement and analysis of photofragment translational energy distributions and recoil anisotropies for the photodissociation of acetophenone at 193 and 248 nm. The photon wavelength of 248 nm falls between the $S_0 \rightarrow S_2$ and $S_0 \rightarrow S_3$ absorption peaks.[15] The previous kinetic study concluded that following $S_0 \rightarrow S_2$ excitation, triplet acetophenone dissociates exclusively into C_6H_5CO(benzoyl radical)$+CH_3$.[15] The absorption cross section for acetophenone at 193 nm is not available. However, judging from the trend of the absorption cross sections measured near 210 nm, the absorption cross section at 193 nm is likely to be much higher than that for the $S_0 \rightarrow S_3$ peak. Excited states higher than S_3 are likely responsible for the photochemistry of acetophenone at 193 nm. In accordance with the known UV photochemistry of ketone,[1–5,10,15] we find that the dissociation of $C_6H_5COCH_3$ at 193 and 248 nm is dominated by processes (1) and (2):

$$C_6H_5COCH_3 + h\nu \rightarrow C_6H_5CO + CH_3 \quad (1)$$

$$\rightarrow C_6H_5 + CH_3CO \quad (2)$$

$$\rightarrow C_6H_5CH_3 + CO. \quad (3)$$

Evidence is found for the very minor occurrence of process (3).

Accurate energetic information about processes (1) and (2) is essential for the analysis of the photofragment TOF spectra observed in this experiment. The heats of formation at 0 K (298 K), $\Delta_fH°_0$ ($\Delta_fH°_{298}$) for the radical fragments formed in processes (1) and (2) are not well established. Thus, we have conducted a theoretical study of the energetics of C_6H_5CO, C_6H_5, and CH_3CO using established *ab initio* quantum chemical schemes, such as the Gaussian 2 (G2) theory and its variances.[16–19] We note that the G2 and G2(MP2) calculations of the heat of formation for the acetyl radical have been reported previously.[20] The errors associated with G2 predictions for $\Delta_fH°_0$ ($\Delta_fH°_{298}$) values of larger polyatomic species, such as C_6H_5CO and C_6H_5, may be higher than that of CH_3CO.[20] Recent G2-type schemes, which combine the G2-type calculations and appropriate isodesmic reactions, have been shown to provide accurate $\Delta_fH°_0$ ($\Delta_fH°_{298}$) predictions even for large polyatomic species.[21–24]

II. EXPERIMENTAL AND THEORETICAL METHODS

A. Experiment

The rotatable beam source laser photofragmentation TOF apparatus used in this study has been described in detail.[25–28] The apparatus consists of three main components: an ArF excimer laser, a photodissociation chamber in which

a rotatable supersonic molecular beam intersects with the excimer laser beam, and a linearly movable ultrahigh vacuum electron ionization quadrupole mass spectrometer (QMS).

A continuous molecular beam of $C_6H_5COCH_3$ (about 3% seeded in He) was produced by supersonic expansion through a nozzle (diameter=0.125 mm) at a total stagnation pressure (P_0) of 360 Torr for 193 nm excitation and 560 Torr for 248 nm excitation. For the TOF measurement of C_6H_5 formed at 248 nm and θ_{lab} (the angle between the molecular beam and the detector axis) $= 10°$, P_0 was reduced to 260 Torr in order to minimize the influence of dimers and clusters. The nozzle stagnation temperature (T_0) was maintained at ≈ 180 °C for 193 nm measurements and at ≈ 130 °C for 248 nm measurements. During the experiment, the beam source, differential pumping, and photodissociation chambers were maintained at pressures of $\approx 1 \times 10^{-4}$, 2×10^{-6}, and $\leq 1 \times 10^{-7}$ Torr, respectively.

The energy of the excimer laser (Questek model 2460) used was in the range of 60–80 mJ/pulse at 193 nm or 100–140 mJ/pulse at 248 nm. The laser beam entered the photodissociation chamber through a MgF_2 focusing lens and intersected the seeded $C_6H_5COCH_3$ beam and the central axis of the QMS at 90°. The spot size of the excimer laser beam was estimated to be ≈ 5 mm^2 at the photodissociation region.

The electron energy and emission current of the ionizer used were 75 eV and 1.2 mA, respectively. During the experiment, the ionization chamber pressure was maintained at $\leq 5 \times 10^{-11}$ Torr. Unless specified, the TOF spectra were taken at a flight path (the distance between the photodissociation region and the ionizer) of 65.5 cm. The TOF spectra were recorded on a multichannel scaler (Stanford Research model SRT430), which was usually set to a channel width of 1.28 μs.

The velocity distribution of the parent $C_6H_5COCH_3$ molecular beam was measured by recording the laser hole burning spectra[25,28] at the mass corresponding to $C_6H_5COCH_3^+$, (or $C_6H_5^+$) at $\theta_{lab} = 0°$. The measured speed profile of a species was then fitted to an assumed functional form, $f(v) \sim v^2 \exp[-(v-v_0)^2/\alpha^2]$, where v_0 is the most probable speed and α is a measure of the width of the speed profile.[25,29] For 193 nm excitation, these constants were determined to be $v_0 = 1.79 \times 10^5$ cm/s and $\alpha = 0.91 \times 10^4$ cm/s. In the case of 248 nm excitation, $v_0 = 1.73 \times 10^5$ cm/s and $\alpha = 0.79 \times 10^4$ cm/s for $P_0 = 560$ Torr, while $v_0 = 1.44 \times 10^5$ cm/s and $\alpha = 1.15 \times 10^5$ cm/s for $P_0 = 260$ Torr.

The ion drift times through the quadrupole mass filter were determined in a hole burning experiment. By recording the hole burning spectra[28] of different ions, $C_6H_5COCH_3^+$, $C_6H_5CO^+$, CH_3CO^+, $C_6H_5^+$, and CH_3^+ formed in electron impact ionization of $C_6H_5COCH_3$, the corresponding arrival times (t) and masses (m) of these ions were used to fit the equation: $t = Am^{1/2} + t_0$, where t_0 is the flight time of $C_6H_5COCH_3$ from the photodissociation region to the ionizer and A is a constant. The procedure yielded a value of 4.114 for A. That is, the ion drift time through the QMS is determined as 4.114 m$^{1/2}$ μs. The actual flight times of photofragments were corrected for the corresponding ion drift times.

The analysis of the TOF data was performed by a forward simulation method.[30,31] Briefly, the procedure began with a trial kinetic energy distribution $P(E_{c.m.})$, which was transformed to a TOF spectrum for comparison with the experimental TOF spectrum. Here, $E_{c.m.}$ represents the center-of-mass kinetic energy of the photofragment. The $P(E_{c.m.})$ distribution was adjusted until satisfactory agreement between the experimental and calculated TOF data was obtained. For the determination of the threshold (maximum) $E_{c.m.}$ threshold of a dissociation process, the $P(E_{c.m.})$ distribution near the $E_{c.m.}$ onset was also obtained by direct transformation[25] of the TOF data.

In the measurements of the angular distribution, the laser light was polarized by a stack of ten quartz plates set at the Brewster angle. The electric vector **E** of the polarized laser beam was set perpendicular to the detector and then rotated to the desired angle with a 193 nm (or 248 nm) half-wave retarder. The laser energy was measured by a pyroelectric detector, and was kept at 10 mJ/pulse at 193 nm and 15 mJ/pulse at 248 nm.

B. *Ab initio* calculations

The G2 *ab initio* theoretical procedure has been described in detail by Curtiss *et al.*[16] It effectively corresponds to the QCISD(T)/6-311+G($3df,2p$)//MP2/6-31G(d) level of theory. Briefly, at the G2 level of theory, molecular structures are optimized with the Hartree–Fock (HF) approach and the second-order Møller-Plesset perturbation theory (MP2), with all electrons included using the 6-31G(d) basis set [i.e., at the HF/6-31G(d) and MP2(full)/6-31G(d) levels]. Harmonic vibrational frequencies are calculated at the HF/6-31G(d) geometries for stationary point characterization. All subsequent single-point calculations at higher levels involved are based on the MP2/6-31G(d) optimized structures. Approximations of QCISD(T)/6-311+G($3df,2p$) energies are obtained with frozen-core, single-point calculations at the QCISD(T)/6-311G(d,p), MP4/6-311G(d,p), MP4/6-311 +G(d,p), MP4/6-311G($2df,p$), and MP2/6-311 +G($3df,2p$) levels. A small semiempirical correction is applied to account for high level correlation effects to obtain the total electronic energy (E_e). The HF/6-31G(d) harmonic vibrational frequencies, scaled by 0.8929, are used for zero-point vibrational energy (ZPVE) correction. The total energy at 0 K (E_0) is equal to $E_e + $ZPVE.[32] All calculations are performed on IBM RS6000/90 and SGI Power Indigo 2 (with R10000 cpu) workstations using the GAUSSIAN 94 package of program.[33] Unless specified, the $\Delta_f H^\circ_0$ and $\Delta_f H^\circ_{298}$ values for the molecules are derived by evaluating the atomization energies and using the known experimental $\Delta_f H^\circ_0$ values of C (170.0 kcal/mol), O(^3P) (59.0 kcal/mol), and H (51.63 kcal/mol).[21,32]

The G2(MP2) theory[17] is a variation of the G2 procedure in which the single-point energies are calculated only at the QCISD(T)/6-311G(d,p) and MP2/6-311+G($3df,2p$) levels. In this study, we have obtained E_0[G2(MP2)] values for C_6H_5, CH_3CO, CH_3, and CO. In view of the large size of $C_6H_5COCH_3$ and C_6H_5CO, the QCISD(T)/6-311G(d,p)

single-point energy calculations are computationally very demanding. Here, we have calculated the E_0 values for $C_6H_5COCH_3$, C_6H_5CO, CH_3CO, CH_3, and CO using the approximated G2(MP2,SVP) scheme introduced by Radom and co-workers.[34] In the G2(MP2,SVP) scheme, the QCISD(T)/6-311G+($3df,2p$) energies are calculated using an additivity approximation,

$$E[\text{QCISD(T)}/6\text{-}311\text{G}+(3df,2p)]$$
$$\approx E[\text{QCISD(T)}/6\text{-}31\text{G(d)}]$$
$$+ E[\text{MP2}/6\text{-}311+\text{G}(3df,2p)] - E[\text{MP2}/6\text{-}31\text{G(d)}].$$

$$(4)$$

The G2(MP2,SVP) calculations have been shown to reproduce proton affinities for a set of reference molecules to within the G2 target accuracy of 2 kcal/mol but at significantly lower computational cost. Surprisingly, it is found that G2(MP2,SVP) performs better than G2 for hydrocarbons and radicals.[34,35] Thus, we have applied the G2(MP2,SVP) procedure to calculate the $\Delta_f H^\circ_0$ ($\Delta_f H^\circ_{298}$) values of $C_6H_5COCH_3$, C_6H_5CO, C_6H_5, CH_3CO, CH_3, and CO.

III. RESULTS AND DISCUSSION

A. Thermochemistry

The theoretical E_0, $\Delta_f H^\circ_0$, and $\Delta_f H^\circ_{298}$ values for $C_6H_5COCH_3$, C_6H_5CO, C_6H_5, CH_3CO, CH_3, and CO obtained here and in previous calculations[20,32] at the G2, G2(MP2), and G2(MP2,SVP) levels of theory are compared with the experimental[21,22,36] values in Table I. In the case when only the $\Delta_f H^\circ_0$ ($\Delta_f H^\circ_{298}$) value for a species is known, the corresponding $\Delta_f H^\circ_{298}$ ($\Delta_f H^\circ_0$) value is obtained using the calculated HF/6-31G(d) vibrational frequencies.

The $\Delta_f H^\circ_0$ (-0.55 ± 0.6 kcal/mol) and $\Delta_f H^\circ_{298}$ (-2.2 ± 0.6 kcal/mol) values for CH_3CO have been determined at high levels of theory using an isodesmic reaction.[20] This calculation supports the recent experimental $\Delta_f H^\circ_{298}$ value of -2.39 ± 0.29 kcal/mol for CH_3CO.[22] The $\Delta_f H^\circ_0$ ($\Delta_f H^\circ_{298}$) values calculated for CH_3CO following the normal G2, G2(MP2), and G2(MP2,SVP) procedures are in satisfactory agreement with those of Ref. 20, with the G2(MP2,SVP) $\Delta_f H^\circ_0$ ($\Delta_f H^\circ_{298}$) value closest to the experimental finding. In a recent study of the C–H bond energy of benzene, values of 84.3 ± 0.6 and 81.2 ± 0.6 kcal/mol are recommended for $\Delta_f H^\circ_0(C_6H_5)$ and $\Delta_f H^\circ_{298}(C_6H_5)$, respectively.[36] These latter values are significantly lower than the corresponding G2(MP2) $\Delta_f H^\circ_0$ (93.0 kcal/mol) and $\Delta_f H^\circ_{298}$ (90.3 kcal/mol) values for C_6H_5. It is known that there is an accumulation of errors in the application of G2-type approaches to larger molecules.[34,35,37,38] For example, the $\Delta_f H^\circ_0$ and $\Delta_f H^\circ_{298}$ values for benzene (C_6H_6) are too low compared to known experimental values by 3.9 and 5.1 kcal/mol, respectively.[34,38] It is interesting that the $\Delta_f H^\circ_0$[G2(MP2,SVP)] (86.1 kcal/mol) and $\Delta_f H^\circ_{298}$[G2(MP2,SVP)] (83.4 kcal/mol) values for C_6H_5, though still higher, are in better agreement with the experimental values. This observation is consistent with the previ-

TABLE I. E_0[G2(MP2)], $\Delta_f H°_0$[G2(MP2)], $\Delta_f H°_{298}$[G2(MP2)], $\Delta_f H°_0$[G2(MP2,SVP)], $\Delta_f H°_{298}$[G2(MP2,SVP)], and $\Delta_f H°_0$(expt) values for $C_6H_5COCH_3$, C_6H_5CO, C_6H_5, CH_3CO, and CH_3.

	Theory[a]			Experiment[b]	
Species	E_0 (hartree)	$\Delta_f H°_0$ (kcal/mol)	$\Delta_f H°_{298}$ (kcal/mol)	$\Delta_f H°_0$ (kcal/mol)	$\Delta_f H°_{298}$ (kcal/mol)
$C_6H_5COCH_3$	−384.187 95	−18.6[c]	−23.4[c]	−15.9	−20.7±0.4
$C_6H_5CH_3$	---	---	---	17.5±0.1	12.0±0.1
C_6H_5CO	−344.309 82	30.3[c]	27.8[c]	29±2[d]	26.1±2[d]
		33.9±1.3[g]	30.6±0.7[g]	33.3±2.2[h]	29.4±2.3[h]
C_6H_5	−231.091 98	93.0[e]	90.3[e]	84.3±0.6	81.2±0.6
	−231.093 71	86.1[c]	83.4		
		87.6±1.0[g]	84.5±0.6[g]		
CH_3CO	−152.935 46[d]	−1.3[f]		−0.74±0.29	−2.39±0.29[i]
		−0.55±0.6[j]	−2.2±0.6[j]		
	−152.931 56	−1.5[e]			
	−152.930 13	−1.7[c]	−2.85[c]		
CH_3	−39.743 90	35.7[f]	35.1[f]	35.8±0.1	35.0±0.1
	−39.736 95	36.2[e]	35.6[e]		
	−39.742 15	36.3[c]	35.7[c]		
CO	−113.177 49	−29.0[f]	−28.2[f]	−27.20±0.04	−26.4±0.0
	−113.175 40	−30.1[e]	−29.3[c]		
	−113.175 71	−30.4[c]	−29.6[c]		

[a]The theoretical $\Delta_f H°_0$ and $\Delta_f H°_{298}$ values are calculated using the $\Delta_f H°_0$(expt) values of C(170.0 kcal/mol), O(^3P) (59.0 kcal/mol), and H (51.63 kcal/mol) from Ref. 21, and theoretical E_0 values calculated at the G2, G2(MP2), or G2(MP2,SVP) level.
[b]Unless specified, experimental values are from Ref. 21.
[c]G2(MP2,SVP) values.
[d]Reference 23.
[e]G2(MP2) values.
[f]G2 values.
[g]Calculated using isodesmic reactions of Table II.
[h]This work.
[i]Reference 22.
[j]Reference 20. Calculated using an isodesmic reaction.

ous finding that G2(MP2,SVP) performs better than G2 for hydrocarbons and radicals.[35]

It has been demonstrated that more accurate heats of formation can be calculated by the use of isodesmic reactions rather than atomization energies as in standard G2-type procedures.[34,37,38] The cancellation of errors in cases involving similar chemical bonds improves the agreement with experiment. In G2-type approaches, a semiempirical high level correction is involved. It was pointed out that the high level corrections can be canceled exactly for isodesmic schemes.[38] In order to obtain reliable theoretical $\Delta_f H°_0$($\Delta_f H°_{298}$) values for C_6H_5CO and C_6H_5, we have examined the variation of their calculated $\Delta_f H°_0$($\Delta_f H°_{298}$) values at the G2(MP2) and G2(MP2,SVP) level by the use of selected isodesmic reactions shown in Table II. We find that for reactions involving radicals, such as C_6H_5CO and C_6H_5, the ''bond separation'' isodesmic reactions are not unique (see Table II, reactions i–iii for C_6H_5 and reactions v–viii for C_6H_5CO).[38] These reactions are selected because the energetics of all species involved are well known, except those for C_6H_5CO and C_6H_5. The uncertainties for $\Delta_f H°_0$($\Delta_f H°_{298}$) thus determined using individual isodesmic reactions are lower limits determined only by the uncertainties of the experimental $\Delta_f H°_0$($\Delta_f H°_{298}$) values used in the calculations. We have also calculated the G2(MP2,SVP) $\Delta_f H°_0$($\Delta_f H°_{298}$) values

of C_6H_5 and C_6H_5CO using isodesmic reactions iv and ix, respectively, (see Table II). As shown in the table, the $\Delta_f H°_0$($\Delta_f H°_{298}$) values of C_6H_5 and C_6H_5CO, thus derived, are highly consistent with the maximum deviations of 1.3 and 2.2 kcal/mol for $\Delta_f H°_0$($\Delta_f H°_{298}$) of C_6H_5 and C_6H_5CO, respectively. We recommend the average values 87.6 ±1.0(84.5±0.6)kcal/mol for $\Delta_f H°_0$($\Delta_f H°_{298}$) of C_6H_5 and 33.9±1.3(30.6±0.7)kcal/mol for $\Delta_f H°_0$($\Delta_f H°_{298}$) of C_6H_5CO. We have conservatively assigned the uncertainties to be the maximum of the differences between individually calculated $\Delta_f H°_0$($\Delta_f H°_{298}$) values and the corresponding averages. Again, we note that these recommended $\Delta_f H°_0$($\Delta_f H°_{298}$) values for C_6H_5 and C_6H_5CO are in reasonable agreement with the $\Delta_f H°_0$[G2(MP2,SVP)] and $\Delta_f H°_{298}$[G2(MP2,SVP)] predictions. Comparing these values and the experimental results (Table I) indicates that the literature $\Delta_f H°_0$($\Delta_f H°_{298}$) values for C_6H_5 and C_6H_5CO are likely on the low side.

In Table III, we have compared the theoretical G2(MP2,SVP) and experimental D_0(D_{298}) values for the C_6H_5CO–CH_3, C_6H_5–$COCH_3$, C_6H_5–CO, and CH_3–CO bonds. The experimental D_0(D_{298}) values for the C_6H_5CO–CH_3 and C_6H_5–$COCH_3$ bonds are 4.4 (5.0) and 2.3 (4.4) kcal/mol lower than the corresponding theoretical

TABLE II. Values for $\Delta_f H^\circ_0$ and $\Delta_f H^\circ_{298}$ of C_6H_5 and C_6H_5CO calculated using selected isodesmic reactions.[a]

	G2(MP2)		G2(MP2,SVP)	
Isodesmic reactions	$\Delta_f H^\circ_0$ (kcal/mol)	$\Delta_f H^\circ_{298}$ (kcal/mol)	$\Delta_f H^\circ_0$ (kcal/mol)	$\Delta_f H^\circ_{298}$ (kcal/mol)
C_6H_5				
i. $C_6H_5 + 6CH_4 \rightarrow 2C_2H_4 + C_2H_3 + 3C_2H_6$	88.2 ± 0.9	84.8 ± 0.9	88.0 ± 0.9	84.6 ± 0.9
ii. $C_6H_5 + 6CH_4 + 3C_2H_4 + C_2H_5 + 2C_2H_6$	87.3 ± 0.3	84.3 ± 0.3	86.4 ± 0.3	83.9 ± 0.3
iii. $C_6H_5 + 7CH_4 \rightarrow 3C_2H_4 + 3C_2H_6 + CH_3$	88.6 ± 0.4	85.1 ± 0.4	87.4 ± 0.4	84.6 ± 0.4
iv. $C_6H_5 - COCH_3 + CH_4 \rightarrow C_6H_5 + CH_3 - COCH_3$			87.0 ± 0.5	84.2 ± 0.5
C_6H_5CO				
v. $C_6H_5CO + 8CH_4 \rightarrow 2C_2H_4 + C_2H_3 + 4C_2H_6 + H_2CO$			34.6 ± 0.9	31.0 ± 0.9
vi. $C_6H_5CO + 8CH_4 \rightarrow 3C_2H_4 + C_2H_5 + 3C_2H_6 + H_2CO$			33.5 ± 0.4	30.3 ± 0.4
vii. $C_6H_5CO + 8CH_4 \rightarrow 3C_2H_4 + 4C_2H_6 + HCO$			34.2 ± 0.4	30.6 ± 0.4
viii. $C_6H_5CO + 9CH_4 \rightarrow 3C_2H_4 + 4C_2H_6 + H_2CO + CH_3$			34.8 ± 0.4	31.0 ± 0.4
xi. $C_6H_5CO - CH_3 + CH_3 \rightarrow C_6H_5CO + H_3C - CH_3$			32.6 ± 0.4	29.9 ± 0.4

[a]$\Delta_f H^\circ_0$(expt) and $\Delta_f H^\circ_{298}$(expt) values used are from Refs. 21 and 35.

predictions, while the experimental $D_0(D_{298})$ values for the $C_6H_5 - CO$ and $CH_3 - CO$ bonds are higher than the respective theoretical predictions by 4.8 (3.2) and 1.5 (1.7) kcal/mol.

B. Newton diagrams for photodissociation at 193 and 248 nm

Based on the conservation of energy,

$$E(h\nu) + E_{int}(C_6H_5COCH_3)$$
$$= D_0(C_6H_5CO - CH_3 \text{ or } C_6H_5 - COCH_3)$$
$$+ E_{int}[(C_6H_5CO + CH_3) \text{ or } C_6H_5 + CH_3CO] + E_{c.m.},$$
$$(5)$$

where $E(h\nu)$ is the dissociation photon energy (147.9 kcal/mol for $h\nu = 193.3$ nm and 115.3 kcal/mol for $h\nu = 248$ nm); and E_{int} is the initial internal energy of $C_6H_5COCH_3$ or its photofragments ($C_6H_5CO + CH_3$ or $C_6H_5 + COCH_3$). Using the HF/6-31G(d) vibrational frequencies for $C_6H_5COCH_3$, the total thermal energy at 298 K for $C_6H_5COCH_3$ is estimated to be 5.7 kcal/mol. Considering the mild expansion conditions used in this experiment, we expect that the vibrational relaxation is inefficient and the rotational relaxation is incomplete. For an initial nozzle temperature of 130–180 °C (403–453 K), we estimate that the effective beam temperature for $C_6H_5COCH_3$ is most likely in the range of 250–350

K. Thus, after expansion, the parent $C_6H_5COCH_3$ molecules may contain ≈ 5.7 kcal/mol of thermal energy.

Using Eq. (5) and the literature D_0 values [$D_0(C_6H_5CO - CH_3) = 80.7$ kcal/mol and $D_0(C_6H_5 - COCH_3) = 99.5$ kcal/mol] (see Table III), we have constructed the Newton diagrams for the $C_6H_5CO + CH_3$ and $C_6H_5 + COCH_3$ channels. The Newton diagrams corresponding to 193 and 248 nm photodissociation are shown in Figs. 1(a) and 1(b), respectively, where v_{lab} and $v_{c.m.}$ are the laboratory and center-of-mass velocities for the photofragments, and θ_{lab} and $\theta_{c.m.}$ are the laboratory and center-of-mass angles, defined by the angles between the detector axis and molecular beam axis and between $v_{c.m.}$ and the molecular beam axis, respectively. The v_0 values are 1.79×10^5 cm/s for 193 nm excitation and 1.73×10^5 cm/s for 248 nm excitation. The maximum $v_{c.m.}$ circles are calculated assuming $E_{int}[(C_6H_5CO + CH_3) \text{ or } (C_6H_5 + CH_3CO)] = 0$. Also shown in Figs. 1(a) and 1(b) are γ and ϵ, which are defined as the angles between the laser electric field **E** and $v_{c.m.}$ and between **E** and the detector axis, respectively.

C. Photodissociation at 193 nm

Figures 2(a) and 2(b) show the TOF spectra for CH_3 observed at $\theta_{lab} = 15°$ and $30°$, respectively. The TOF spectrum for C_6H_5CO at $\theta_{lab} = 15°$ is depicted in Fig. 3. The

TABLE III. Comparison of theoretical and experimental selected bond dissociation energies at 0 (298 K) for $C_6H_5COCH_3$, C_6H_5CO, and CH_3CO.[a]

	Theory [G2(MP2,SVP)]		Experiment	
Reactions	D_0 (kcal/mol)	D_{298} (kcal/mol)	D_0 (kcal/mol)	D_{298} (kcal/mol)
$C_6H_5COCH_3 \rightarrow C_6H_5CO + CH_3$	85.1	86.8	80.7	81.8
			85.0 ± 2.2[b]	
$C_6H_5COCH_3 \rightarrow C_6H_5 + CH_3CO$	102.8	103.8	99.5	99.5
$C_6H_5CO \rightarrow C_6H_5 + CO$	23.3	25.5	28.1	28.7
$CH_3CO \rightarrow CH_3 + CO$	6.8	8.2	9.3	11.0

[a]Calculated using the experimental and theoretical G2(M2,SVP) $\Delta_f H^\circ_0(\Delta_f H^\circ_{298})$ values of Table I.
[b]This work.

(a)

(b)
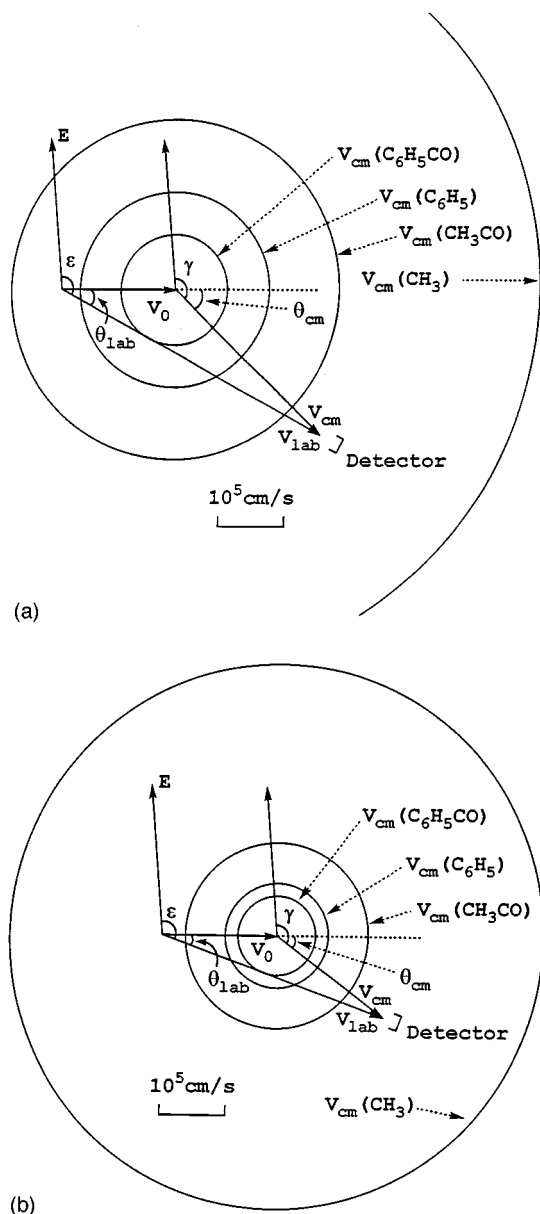
FIG. 1. Kinematics for the formation of $C_6H_5CO+CH_3$ by process (1) and the formation of $C_6H_5+COCH_3$ by process (2) at (a) $h\nu=193$ nm and (b) 248 nm. v_0 is the laboratory velocity for $C_6H_5COCH_3$, and $v_{c.m.}(C_6H_5CO)$, $v_{c.m.}(C_6H_5)$, $v_{c.m.}(CH_3CO)$, and $v_{c.m.}(CH_3)$ are the maximum c.m. velocities for C_6H_5CO, C_6H_5, CH_3CO, and CH_3, respectively. The diagrams show the relationship $\gamma=\theta_{c.m.}+\epsilon-\theta_{lab}$ where γ is the angle between the laser electric field (**E**) and $v_{c.m.}$; $\theta_{c.m.}$ is the angle between v_0 and $v_{c.m.}$; ϵ is the angle between **E** and the detector axis; and θ_{lab} is the angle between the molecular beam axis and the detector axis. The figures show that the maximum θ_{lab} values for the detection of C_6H_5CO are 27.0° for $h\nu=193$ and 19.8° for $h\nu=248$ nm.

direct detection of C_6H_5CO and CH_3 signals confirms the occurrence of process (1). The $P(E_{c.m.})$ for process (1) (solid curve) shown in Fig. 4(a) is derived from the fast peaks in the CH_3 TOF spectra. This $P(E_{c.m.})$ peaks near 12 kcal/mol and has an $E_{c.m.}$ onset of 34 kcal/mol. The latter value is significantly lower than the thermochemical $E_{c.m.}$ threshold of 67 kcal/mol. The average kinetic energy release of 13.8 kcal/mol for process (1) is $\approx 20\%$ of the total available energy.
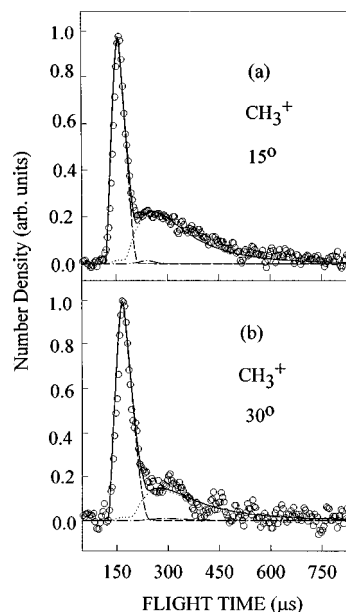
FIG. 2. TOF spectra for CH_3 at (a) $\theta_{lab}=15°$ and (b) $\theta_{lab}=30°$. Circles represent experimental data. Contributions are shown for CH_3 (dashed line) from process (1), CH_3CO (dot-dashed line) from process (2), and CH_3 (dotted line) from process (8).

We attempt to use the $P(E_{c.m.})$ derived from the CH_3 spectrum to fit the TOF spectrum for C_6H_5CO, and find that the $P(E_{c.m.})$ at $E_{c.m.}>15$ kcal/mol [indicated by the dashed curve in Fig. 4(a)] satisfactorily fits the C_6H_5CO TOF spectrum. This observation indicates that a fraction of excited C_6H_5CO radicals initially formed with $E_{c.m.}<15$ kcal/mol [or $E_{int}(C_6H_5CO+CH_5)>52$ kcal/mol] by process (1) undergoes further dissociation in the time scale of the present experiment. If the internal energy distributed in C_6H_5CO and CH_3 is proportional to the internal degrees of freedom, the internal energy for C_6H_5CO is expected to be >41.6 kcal/mol at $E_{c.m.}<15$ kcal/mol. Since the $D_0(C_6H_5-CO)$ is <29 kcal/mol (see Table III), excited C_6H_5CO radicals with internal excitation >29 kcal/mol are expected to dissociate according to
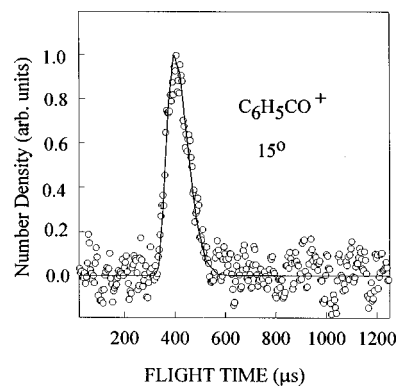
$$C_6H_5CO \rightarrow C_6H_5+CO. \qquad (6)$$

FIG. 3. TOF spectrum for C_6H_5CO at $\theta_{lab}=15°$. Circles represent experimental data.
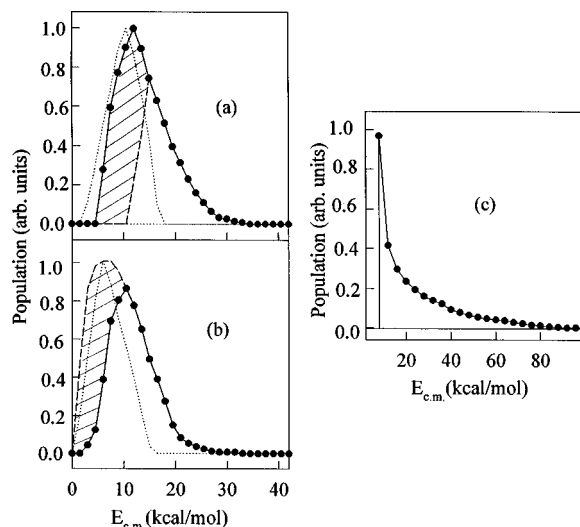
FIG. 4. (a) The $P(E_{c.m.})$ for process (1) derived by the TOF spectra for CH_3 is shown as the solid curve. The part of the $P(E_{c.m.})$ to the right of the dashed line fits the TOF spectrum for C_6H_5CO of Fig. 3. The $P(E_{c.m.})$ for the secondary dissociation process (6) derived by the TOF spectra for C_6H_5 and CO is shown by the dotted line. (b) The solid curve is the approximated $P(E_{c.m.})$ for process (2) derived by the TOF of CH_3CO at $\theta_{lab}=15°$. The modified $P(E_{c.m.})$ for process (2) (dashed curve) at $E_{c.m.}<11$ kcal/mol is obtained by fitting the TOF spectrum for C_6H_5 at $\theta_{lab}=15°$. Thus, the complete $P(E_{c.m.})$ for process (2) is the combined dashed curve at $E_{c.m.}<11$ kcal/mol and the solid curve at $E_{c.m.}\geq11$ kcal/mol. The $P(E_{c.m.})$ for the secondary dissociation of CH_3CO obtained by fitting the slow peak the CH_3 TOF spectra of Figs. 2(a) and 2(b) is shown by the dotted curve. (c) $P(E_{c.m.})$ derived by the TOF spectrum of $C_6H_5CH_3$ of Fig. 8. The TOF spectrum of $C_6H_5CH_3$ does not contain information for $P(E_{c.m.})$ at $E_{c.m.}<8$ kcal/mol due to the kinematic constraint.

On the basis of the $P(E_{c.m.})$'s derived from the TOF spectra of CH_3 and C_6H_5CO, we conclude that $\approx50\%$ of the primary C_6H_5CO radicals [corresponding to the shaded area in Fig. 4(a)] undergoes further dissociation according to process (6).

The TOF spectrum for CH_3CO measured at $\theta_{lab}=15°$ and a flight path of 84.5 cm is shown in Fig. 5(a). We have also observed the TOF spectrum for CH_2CO as shown in Fig. 5(b). Figures 6(a) and 6(b) depict the TOF spectra for C_6H_5 at $\theta_{lab}=15°$ and $30°$, respectively. The observation of the CH_3CO and C_6H_5 spectra indicates the occurrence of process (2). The TOF spectrum for CH_3CO is used to derive the approximated $P(E_{c.m.})$ for process (2), shown as the solid curve in Fig. 4(b). The $P(E_{c.m.})$ thus obtained fits the TOF spectrum for CH_2CO, indicating that the CH_2CO^+ signal arises from the dissociative electron ionization of CH_3CO.

We expect that CH_3^+ fragment ions formed in the dissociative electron ionization of CH_3CO [process (7)] contribute to the TOF spectra for CH_3 (Fig. 2):

$$CH_3CO + e^- \rightarrow CH_3^+ + CO + 2e^-. \tag{7}$$
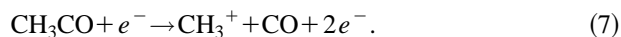
However, the $P(E_{c.m.})$ derived from the TOF spectrum of CH_3CO cannot account for the slow, broad peaks shown in Figs. 2(a) and 2(b). Since $D_0(CH_3-CO)$ is <11 kcal/mol (see Table III), the further dissociation of some internally excited CH_3CO radicals according to process (8) is expected:
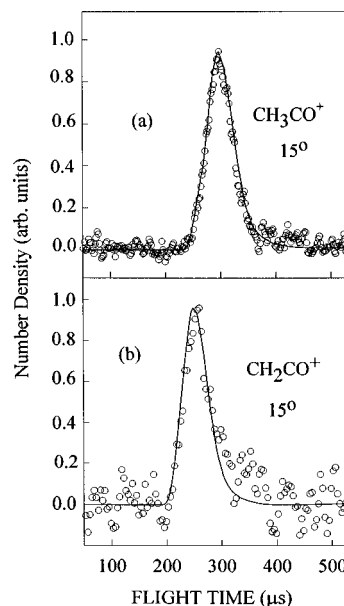

FIG. 5. TOF spectrum for (a) CH_3CO and (b) CH_2CO at $\theta_{lab}=15°$. The spectrum for CH_3CO is measured at a flight path of 84.5 cm. Circles represent the experimental data.

$$CH_3CO \rightarrow CH_3 + CO. \tag{8}$$

Process (8) has been observed for acetyl radicals initially formed in the photodissociation of acetone and acetyl chloride.[1,7] The approximated $P(E_{c.m.})$ for process (2) derived from the TOF spectrum peaks at $E_{c.m.}\approx10.5$ kcal/mol,[39] indicating that the most probable internal energy for $CH_3CO + C_6H_5$ is ≈38 kcal/mol, which is $\approx79\%$ of the available energy. Assuming that this internal energy is partitioned according to the internal degrees of
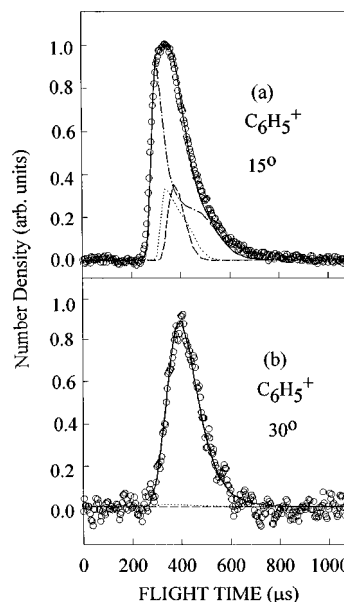

FIG. 6. TOF spectra for C_6H_5 at (a) $\theta_{lab}=15°$ and (b) $\theta_{lab}=30°$. Circles represent experimental data. Contributions are shown for C_6H_5 (dot-dashed line) from process (2), C_6H_5CO (dashed line) from process (1), and C_6H_5 (dotted line) from process (6).

freedom of the photofragments, the most probable internal energy for CH_3CO is estimated to be 19 kcal/mol, which is above the $D_0(CH_3-CO)$ value of 9.3 kcal/mol (see Table III). Since the portion of excited CH_3CO radicals originally formed by process (2) with internal energy greater than $D_0(CH_3-CO)$ is expected to dissociate according to process (8), the true $P(E_{c.m.})$ at lower $E_{c.m.}$ for process (2) should be higher than that indicated by the approximated $P(E_{c.m.})$ derived by the TOF spectrum of CH_3CO. However, the high $E_{c.m.}$ portion of the approximated $P(E_{c.m.})$ based on the CH_3CO spectrum represents the true $P(E_{c.m.})$ for process (2). The $E_{c.m.}$ onset of ≈ 35 kcal/mol observed is more than 10 kcal/mol lower than the thermochemical $E_{c.m.}$ threshold 48.5 kcal/mol for process (2).

Using the secondary $P(E_{c.m.})$ shown as the dotted curve in Fig. 4(b) for the dissociation process (8), we find that the slow, broad peaks observed in the TOF spectra of CH_3 at $\theta_{lab}=15°$ and $30°$ are satisfactorily accounted for by process (8) [see dotted curves in Figs. 2(a) and 2(b)]. We note that the secondary $P(E_{c.m.})$ for process (8) thus obtained peaks at 6 kcal/mol, and is similar to that derived in the 193 nm photodissociation study of acetone.[7] This latter observation can be taken as support for the present attribution of the slow peaks of Figs. 2(a) and 2(b). Based on this attribution, the contribution due to the dissociative electron ionization process (7) is small [see dot-dashed curve in Figs. 2(a) and 2(b)]. The simulation of the CH_3 spectra reveals that the cross sections for process (1) to (2) at $h\nu=193$ nm are comparable.

As a result of the kinematic constraint, C_6H_5CO cannot be observed beyond $27°$ [see Fig. 1(a)]. Thus, $C_6H_5^+$ ions formed in the dissociative electron ionization process (9),

$$C_6H_5CO+e^-\rightarrow C_6H_5{}^+ + CO + 2e^-, \qquad (9)$$

should not contribute to the TOF spectrum for C_6H_5 at $30°$ shown in Fig. 6(b). We find that this latter spectrum can be accounted for by the $P(E_{c.m.})$ derived from the CH_3CO spectrum [Fig. 4(b)] at $E_{c.m.}\geqslant16.5$ kcal/mol. However, the TOF spectrum for C_6H_5 at $15°$, shown in Fig. 6(a), may contain contributions from the primary process (2), the secondary dissociation process (6), and the dissociative electron ionization process (9). The fitting due to processes (2) and (9) are fixed by the $P(E_{c.m.})$'s of the primary processes (1) and (2). The fact that the spectrum of Fig. 6(a) cannot be fitted by processes (2) and (9) indicates the occurrence of secondary process (6). As pointed out above, the approximated $P(E_{c.m.})$ of process (2) derived from the TOF spectrum for CH_3CO represents only the stable part of CH_3CO formed by process (2). The complete $P(E_{c.m.})$ for process (2) should include the secondary dissociation part according to process (8). Therefore, we have adjusted the approximated $P(E_{c.m.})$ at lower $E_{c.m.}$ values to fit the TOF spectrum for C_6H_5 at $15°$. The best fit is achieved by taking into account contributions from process (2) (dot-dashed curve), process (6) (dotted curve), and process (9) (dashed curve). The secondary $P(E_{c.m.})$ used for process (6) (dotted curve) is shown in Fig. 4. The complete $P(E_{c.m.})$ for process (2) [Fig. 4(b)] is thus the combined dashed curve at $E_{c.m.}<10.5$ kcal/mol and the solid

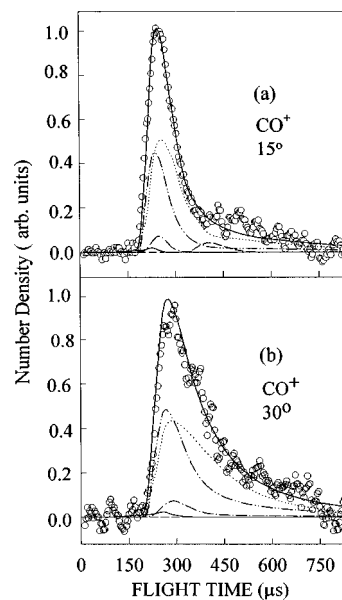FIG. 7. TOF spectra for CO at (a) $\theta_{lab}=15°$ and (b) $\theta_{lab}=30°$. Circles represent experimental data. Contributions are shown for C_6H_5CO (dashed line) from process (1), CH_3CO (dash-dotted line) from process (2), CO (solid line) from process (3), CO (dot-dot-dashed line) from process (6), and CO (dotted) from process (8).

curve at $E_{c.m.}\geqslant10.5$ kcal/mol. The shaded area between the solid and dashed curve represents the portion of excited CH_3CO ($\approx40\%$) undergoing further dissociation. We note that the portion of the $P(E_{c.m.})$ at $E_{c.m.}<10.5$ kcal/mol derived by fitting the C_6H_5 spectrum of Fig. 6(a) has considerable uncertainties. Nevertheless, the fitting of the C_6H_5 spectrum at $15°$ is consistent with the conclusion obtained in the simulation of the TOF spectra for CH_3: the cross sections for processes (1) and (2) are comparable.

Figures 7(a) and 7(b) show the TOF spectra for CO observed at $\theta_{lab}=15°$ and $30°$. In addition to contributions from the secondary dissociation processes (6) and (8), the TOF spectra for CO also contain contributions from the primary processes (1) and (2) due to the dissociative electron ionization processes (10) and (11), respectively:

$$C_6H_5CO+e^-\rightarrow C_6H_5+CO^+ +2e^-, \qquad (10)$$

$$CH_3CO+e^-\rightarrow CH_3+CO^+ +2e^-. \qquad (11)$$
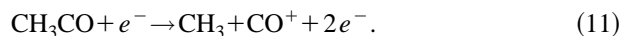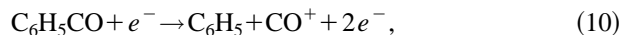
Contributions from processes $(1)+(10)$ (dashed line) and processes $(2)+(11)$ (dot-dashed line) are found to be small. This can be understood by the low efficiencies for CO^+ production in processes (10) and (11) as a result of the significantly higher IE(CO) value than those for C_6H_5 and CH_3.[21] The gross features of the CO TOF spectra of Figs. 7(a) and 7(b) can be fitted by adjusting the portions of process (6) (long dashed line) and process (8) (dotted line).

Figure 8 the TOF spectrum for toluene ($C_6H_5CH_3$) at $15°$ obtained by more than one million laser shots. The direct detection of ($C_6H_5CH_3$) can be taken as evidence that process (3) also occurs. Since the breakage of the CH_3-CO and C_6H_5-CO bonds is compensated by the formation of the $C_6H_5-CH_3$ bond (see Table I for the $\Delta H°_0$ value of
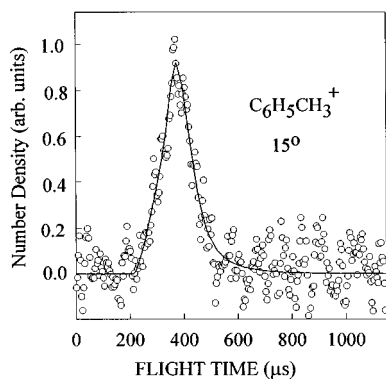
FIG. 8. TOF spectrum for $C_6H_5CH_3$ at $\theta_{lab} = 15°$. Circles represent experimental data. This spectrum was obtained from more than one million laser shots.

FIG. 9. (a) TOF spectra for CH_3 at $\theta_{lab} = 15°$ and $\epsilon = 0°$, $40°$, $90°$, and $130°$. (b) TOF spectra for C_6H_5 at $\theta_{lab} = 15°$ and $\epsilon = 0°$, $20°$, $50°$, $70°$, $100°$, and $150°$.

$C_6H_5CH_3$) and an additional π-bond in CO, the endothermicity at 0 K for process (3) is only 6.2 kcal/mol. However, the activation energy for this dissociation process, which necessarily involves a tight transition complex, is likely to be high. The $P(E_{c.m.})$ for process (3) derived from the TOF spectrum for $CH_3C_6H_5$ is shown in Fig. 4(c). This $P(E_{c.m.})$ decreases rapidly as $E_{c.m.}$ is increased from $E_{c.m.} = 8$ kcal/mol toward higher $E_{c.m.}$, exhibiting the feature expected of a statistical dissociation process. Due to the kinematic constraint, the TOF spectrum for $C_6H_5CH_3$ at $15°$ contains no information for the $P(E_{c.m.})$ at $E_{c.m.} < 8$ kcal/mol. The $E_{c.m.}$ onset for the $P(E_{c.m.})$ of process (3) is >90 kcal/mol. Comparing the observed $C_6H_5CH_3$, C_6H_5, and CH_3 signals, we estimate the cross section for process (3) is $<0.1\%$ of those for processes (1) and (2) at $h\nu = 193$ nm. The contribution of process (3) to the TOF spectra for CO at $15°$ and $30°$ is negligibly small [see the small solid curves in Figs. 7(a) and 7(b)]. The statistical appearance of the $P(E_{c.m.})$ for process (3) is consistent with the long time scale involved in the CH_3 rearrangement for the formation of $C_6H_5CH_3$ from $C_6H_5COCH_3$.

The angular distribution of the photodissociation fragments has the form:[40,41]

$$P(\gamma) = (1/4\pi)[1 + \beta P_2(\cos \gamma)], \qquad (12)$$

where $P_2(\cos \gamma)$ is the second Legendre polynomial and β is the anisotropy parameter. We have measured the TOF spectra for $C_6H_5^+$ at polarization angles $\varepsilon = 0°$, $20°$, $50°$, $70°$, $100°$ and $150°$ and TOF spectra for CH_3^+ at $\varepsilon = 0°$, $40°$, $90°$, $130°$ (Fig. 9). Within experimental error limits, no difference in the spectra is observed. Therefore, we conclude that the photofragment angular distributions for processes (1) and (2) at $h\nu = 193$ nm are isotropic, i.e., $\beta = 0$. This observation is consistent with the conclusion that the 193 nm photodissociation of acetophenone involves a predissociation mechanism with a dissociation lifetime longer than the rotational period of photoexcited $C_6H_5COCH_3$.

D. Excitation at 248 nm

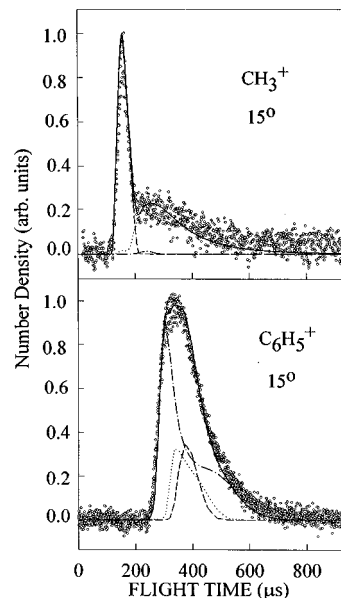Upon the absorption of a 248 nm photon, $C_6H_5COCH_3$ may dissociate according to processes (1) and (2). Since a

248 nm photon corresponds to an energy of 115.2 kcal/mol, and the dissociation of $C_6H_5COCH_3$ into $C_6H_5 + CO + CH_3$ requires 110 kcal/mol, finite dissociation of excited primary C_6H_5CO and CH_3CO radicals according to processes (6) and (8) are still possible. Thus, we have searched for the TOF signals of C_6H_5CO, $C_6H_5CH_3$, C_6H_5, CH_3CO, CH_3, and CO as in the 193 nm photodissociation experiment described above.

However, the measurements of the TOF spectra for C_6H_5CO, CH_3CO, and CH_2CO were unsuccessful despite a long and careful search for $C_6H_5CO^+$, CH_3CO^+, and CH_2CO^+ signals at $\theta_{lab} = 15°$, $20°$, $25°$, and $30°$. The absorption cross section of $C_6H_5COCH_3$ at 248 nm is more than 10% of that at 193 nm.[10,15] Thus, the intensities for C_6H_5CO and CH_3CO at 248 nm are much lower than those at 193 nm. The dissociative ionization processes (7) and (9) are expected to reduce the CH_3CO^+ and $C_6H_5CO^+$ signals. Hoping to minimize the effect of processes (7) and (9), we have also searched for the CH_3CO^+ and $C_6H_5CO^+$ signals at ionizing electron energies lower than 75 eV. However, under such conditions, the signals for CH_3CO^+ and $C_6H_5CO^+$ are too weak to measure the TOF spectra of C_6H_5CO and CH_3CO.

The TOF spectra for CH_3 at $\theta_{lab} = 15°$, $20°$, and $30°$ are depicted in Figs. 10(a), 10(b), and 10(c), respectively. Figures 11(a), 11(b), 11(c), and 11(d) show the respective TOF spectra for C_6H_5 at $\theta_{lab} = 10°$, $15°$, $20°$, and $25°$. The TOF spectra for CO and C_6H_5CO are shown in Figs. 12(a) and 12(b), respectively. We note that the TOF spectra for C_6H_5 at $\theta_{lab} = 25°$, $C_6H_5CH_3$ at $\theta_{lab} = 20°$, CO at $\theta_{lab} = 20°$ result from the accumulation of more than one million laser shots.

Because of the kinematic constraint, C_6H_5CO produced by process (1) cannot be observed at $\theta_{lab} > 20°$ [see Fig. 1(b)]. Thus, the translational energy distribution for process
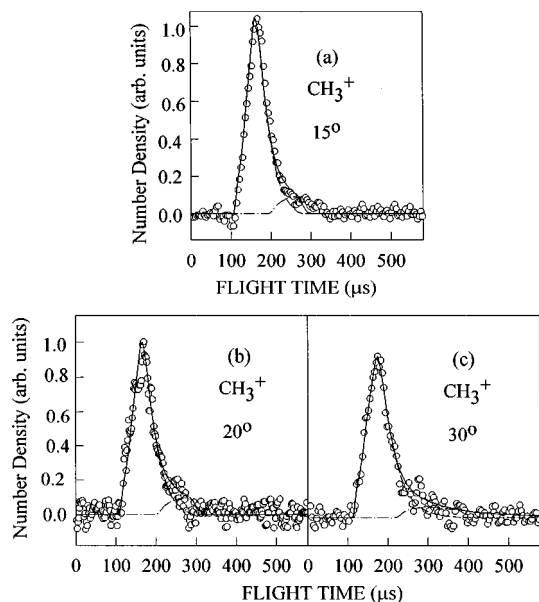
FIG. 10. TOF spectra for CH_3 at (a) $\theta_{lab}=15°$, (b) $\theta_{lab}=20°$, and (c) $\theta_{lab}=30°$. Circles represent experimental data. Contributions are shown for CH_3 (dashed curve) from process (1) and CH_3CO (dot-dashed curve) from process (2).

FIG. 12. (a) TOF spectra for CO at $\theta_{lab}=20°$. Circles represent experimental data. Contributions are shown from CH_3CO (dot-dashed line) formed in process (2) and CO (dashed line) from process (3). (b) TOF spectrum for $C_6H_5CH_3$ at $\theta_{lab}=20°$. Circles represent experimental data. Both spectra were obtained from more than one million laser shots.

(2) at 248 nm can be derived from the TOF spectrum for C_6H_5 at $\theta_{lab}=25°$. However, in this spectrum a very fast onset appears as a shoulder, which cannot be due to process (2) based on the known $D_0(C_6H_5-COCH_3)$. We have attributed this to $C_6H_5^+$ formed in the dissociative electron ionization of $C_6H_5CH_3$. The $P(E_{c.m.})$ for process (2) at $h\nu=248$ nm derived from the TOF spectrum for C_6H_5 at 25° is shown in Fig. 13(b), which increases monotonically as $E_{c.m.}$ is decreased from the onset at $E_{c.m.}\approx19$ to $E_{c.m.}=6$ kcal/mol.
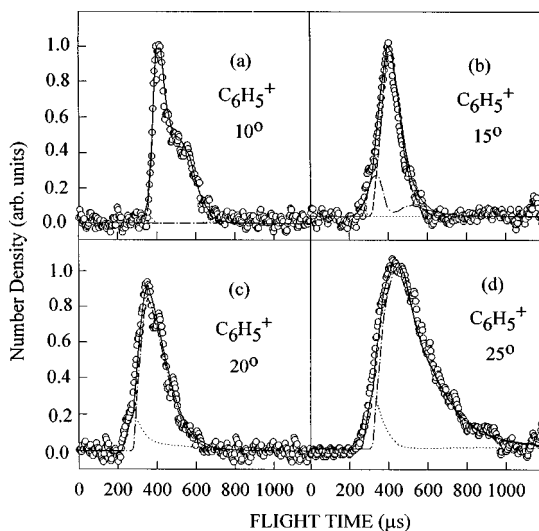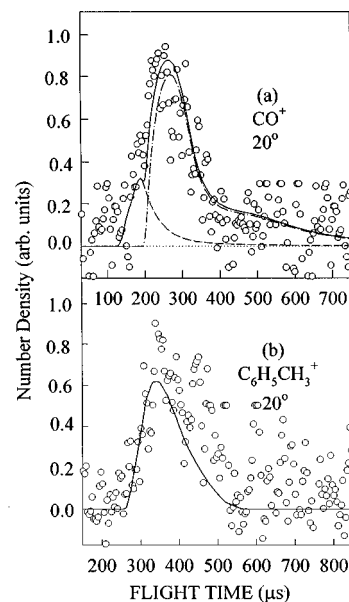
Due to the overlap with the $C_6H_5^+$ signal from $C_6H_5CH_3$, the $E_{c.m.}$ onset for the $P(E_{c.m.})$ of process (2) cannot be determined. The onset for the $P(E_{c.m.})$ of Fig. 13(b) is fixed by the known $D_0(C_6H_5-COCH_3)$ of 99.5 kcal/mol and the estimated thermal energy of ≈4.8 kcal/mol for parent $C_6H_5COCH_3$. The spectrum for C_6H_5 at 25° provides information only about the $P(E_{c.m.})$ at $E_{c.m.}\geqslant6$ kcal/mol. As shown in the analysis below, the $C_6H_5^+$ signal observed at $\theta_{lab}\leqslant15°$ results overwhelmingly from the dissociative electron ionization of C_6H_5CO, i.e., processes (1)+(9). Thus, the

FIG. 11. TOF spectra for C_6H_5 at (a) $\theta_{lab}=10°$, (b) $\theta_{lab}=15°$, and (c) $\theta_{lab}=20°$, and (d) $\theta_{lab}=25°$. The TOF spectrum for C_6H_5 at $\theta_{lab}=25°$ was obtained from more than one million laser shots. Circles represent experimental data. Contributions are shown for C_6H_5CO (dashed curve) from process (1), C_6H_5 (dot-dash curve) from process (2), and $C_6H_5CH_3$ (dotted curve) process (3).
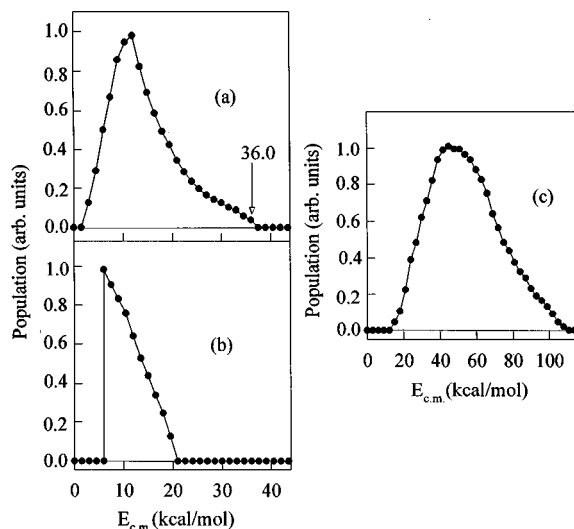

FIG. 13. (a) $P(E_{c.m.})$ for process (1) derived by fitting TOF spectra for CH_3. (b) $P(E_{c.m.})$ for process (2) derived by fitting the TOF spectra for C_6H_5. (c) $P(E_{c.m.})$ for process (3) derived by fitting the TOF spectra for $C_6H_5CH_3$.

TOF spectrum for C_6H_5 at smaller θ_{lab}'s does not provide reliable information about the $P(E_{c.m.})$ for process (2) at $E_{c.m.} < 6$ kcal/mol.

On the basis of the $P(E_{c.m.})$ for process (2) shown in Fig. 13(b), we conclude that the CH_3^+ signal originating from the dissociative electron ionization of CH_3CO [process (7)] contributes only a small component to the tail of the CH_3 spectra of Figs. 10(a)–10(c). Thus, the $P(E_{c.m.})$ for process (1) can be reliably determined from the TOF spectra of CH_3. The $P(E_{c.m.})$ of process (1) thus determined is shown in Fig. 13(a), and peaks near 12 kcal/mol. The average $E_{c.m.}$ energy release is 14.6 kcal/mol, which corresponds to 42% of the available energy of ≈ 35 kcal/mol. The $E_{c.m.}$ onset for the $P(E_{c.m.})$ of process (1) is 36.0 ± 1.5 kcal/mol. Since this experiment uses a nozzle temperature of 130 °C (403 K), the onset observed here is affected by the hot band effect. Without consideration of the hot band effect, we determine a lower bound of 79.3 kcal/mol for $D_0(C_6H_5CO-CH_3)$. Using the HF/6-31G(d) vibrational frequencies, the thermal energy for $C_6H_5COCH_3$ at 403 K is estimated to be 9.5 kcal/mol. Thus, the true $D_0(C_6H_5CO-CH_3)$ value should fall in the range of 79.3–88.8 kcal/mol. As mentioned above, we estimate that the effective temperature for $C_6H_5COCH_3$ after the mild beam expansion is in the range of 250–350 K, corresponding to a thermal energy range of 4.2–7.4 kcal/mol. Taking into account the thermal energy for $C_6H_5COCH_3$, we arrive at a value of 85.0 ± 2.2 kcal/mol for $D_0(C_6H_5CO-CH_3)$. The uncertainties of ± 2.2 kcal/mol given for $D_0(C_6H_5CO-CH_3)$ include the uncertainties of the $E_{c.m.}$ onset and the possible spread in the thermal energy of the parent $C_6H_5COCH_3$. The $D_0(C_6H_5CO-CH_3)$ value obtained here is between the literature value of 80.7 and the theoretical value of 85.1 kcal/mol (see Table III). Using $D_0(C_6H_5CO-CH_3) = 85.0 \pm 2.2$ determined here, together with the known $\Delta_f H°_0(C_6H_5COCH_3) = -15.9 \pm 0.4$ and $\Delta_f H°_0(CH_3) = 35.8 \pm 0$ (see Table I), we obtain $\Delta_f H°_0(C_6H_5CO) = 33.3 \pm 2.2$ kcal/mol, which is in excellent agreement with the value of 33.9 ± 0.4 kcal/mol calculated based on the selected set of isodesmic reactions (see Table I and reactions v–xi in Table II).

The $P(E_{c.m.})$'s for process (1) and (2) of Figs. 13(a) and 13(b) have been used successfully to fit the TOF spectra for C_6H_5 at $\theta_{lab} = 10°$, 15°, and 20° [Figs. 11(a), 11(b), and 11(c)]. The TOF spectrum for C_6H_5 at $\theta_{lab} = 20°$ is mostly due to process (2), with minor contribution from process (3), whereas the TOF spectra for C_6H_5 at $\theta_{lab} = 10°$ and 15° are largely due to process (1), with minor contribution from process (2). We note that the contribution of process (2) to the TOF spectrum for C_6H_5 at $\theta_{lab} = 15°$ has a bimodal structure, which results from the forward and backward scattered components of the C_6H_5 fragments.

The simulation of the TOF spectra for CH_3 at $\theta_{lab} = 15°$, 20° and 25° [Figs. 10(a), 10(b), and 10(c)] shows that the branching ratio of process (2) to process (1) is small at 248 nm. This ratio can also be estimated from the simulation of the TOF spectrum for C_6H_5 at $\theta_{lab} = 10°$ [Fig. 11(a)]. As we have shown in a previous photodissociation study of CS_2,[25] the photofragments resulting from photodissociation
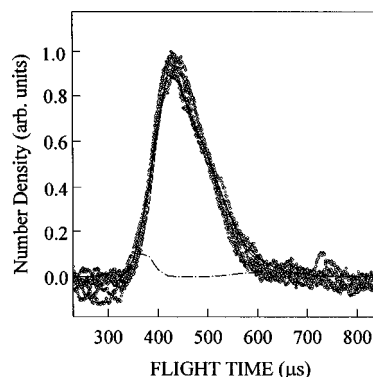

FIG. 14. TOF spectra for C_6H_5 at $\theta_{lab} = 12°$ and $\epsilon = 10°$, 30°, 50°, 70°, 90°, 110°, 130°, 150°, and 170°.

of dimers and clusters are mainly confined to small θ_{lab} values because of kinematic constraints. In order to avoid the influence of dimers and clusters on the TOF measurement at 10°, we have decreased the stagnation pressure of $C_6H_5COCH_3$ to 260 Torr to reduce the effect of supersonic cooling. Under such molecular beam expansion conditions, no signals from electron ionization of dimers and clusters of $C_6H_5COCH_3$ are observed at $\theta_{lab} = 10°$. As shown in Fig. 11(a), the simulation indicates that the TOF spectrum for C_6H_5 at $\theta_{lab} = 10°$ is predominantly accounted for by process (1). On the basis of the simulation of the CH_3 and C_6H_5 TOF spectra, we estimate that the branching ratio of process (2) to process (1) is ≈ 0.01.

The $P(E_{c.m.})$ for process (3) at $h\nu = 248$ nm derived from the TOF spectrum for $C_6H_5CH_3$ [Fig. 12(b)] is depicted in Fig. 13(c). This $P(E_{c.m.})$ is different from that obtained at $h\nu = 193$ nm [Fig. 4(c)]. The observed $E_{c.m.}$ onset of ≈ 106 kcal/mol for the $P(E_{c.m.})$ of Fig. 13(c) is close to the thermochemical threshold of 109 kcal/mol for process (3) at $h\nu = 248$ nm. The $P(E_{c.m.})$ is nearly symmetrical about the maximum at $E_{c.m.} \approx 50$ kcal/mol, indicating that the available energy of 109 kcal/mol for process (3) is about equally partitioned into internal and translational energies of the photofragments. This $P(E_{c.m.})$ of Fig. 13(c) has been used satisfactorily to fit the fast shoulder observed in the TOF spectra for C_6H_5 at $\theta_{lab} = 20°$ and 25° [Figs. 11(c) and 11(d)]. The simulation of the C_6H_5 TOF spectra indicates that the branching ratio for process (2) to process (3) is ≈ 0.08, without considering the difference in the efficiency for the formation of $C_6H_5^+$ by electron ionization of C_6H_5 and that by the dissociative electron ionization of $C_6H_5CH_3$.

Due to the high N_2 background in the ionizer of the QMS, the signal-to-noise ratio is poor for the CO TOF spectrum observed at $\theta = 20°$ [Fig. 14(a)], even after accumulating more than one million laser shots. According to dissociative electron ionization processes (10) and (11), CO^+ from the primary photofragments C_6H_5CO and CH_3CO should also contribute to the CO TOF spectrum. However, as pointed out above, the CO^+ signals from processes (10) and (11) are expected to be small because of the high ionization energy of CO. The simulation of the CO TOF spectrum at $\theta = 20°$ shows that the major contribution is by processes

(2)+(8) (dot-dashed curve), and process (3) contributes as a smaller fast peak (dashed curve). We note that process (1) cannot be seen at $\theta = 20°$ due to the kinematic constraints.

The angular distribution for process (1) is probed by measuring the TOF spectrum for C_6H_5 at $\theta_{lab} = 12°$ and $\epsilon = 10°$, $30°$, $50°$, $70°$, $90°$, $100°$, $130°$, $150°$, and $170°$ (see Fig. 14). These spectra are essentially identical, indicating that the photofragment angular distribution for process (1) is isotropic, i.e., $\beta = 0$. Again, this observation indicates that the dissociation lifetime of the excited state of $C_6H_5COCH_3$ involved is longer than that of the rotational period, and that a predissociation mechanism is operative for process (1) at $h\nu = 248$ nm. Since process (2) is a minor channel, the low TOF signal for CH_3 makes it difficult to measure the photofragment angular distribution for process (2).

IV. CONCLUSION

The TOF spectra for CH_3 and C_6H_5 resulting from the 193 and 248 nm photofragmentation of $C_6H_5COCH_3$ have been measured. At 193 nm, processes (1) and (2) occur with comparable cross sections. The cross section for process (3) at 193 nm is estimated to be $<0.1\%$ of those for processes (1) and (2). Approximately 30–50% of the CH_3CO and C_6H_5CO radicals initially formed at 193 nm by processes (1) and (2) are found to undergo further dissociation according to processes (6) and (8). At 248 nm, process (1) is overwhelmingly the dominant channel. The branching ratios for process (1) : process (2) : process (3) are estimated as 1.0:0.01:0.0008. The energy releases for these dissociation processes have also been determined. The photofragment angular distributions for these processes are isotropic, possibly indicative of a predissociative mechanism. From the $E_{c.m.}$ onset for process (2) at 248 nm, we determine $D_0(C_6H_5CO-CH_3) = 85.0 \pm 2.2$ kcal/mol and $\Delta_f H°_0(C_6H_5CO) = 33.3 \pm 2.2$ kcal/mol.

We have also conducted an *ab initio* study of the energetics for C_6H_5CO, and C_6H_5 formed in processes (1) and (2) using the G2-type procedures together with isodesmic reaction scheme. The theoretical value $\Delta_f H°_0(C_6H_5CO) = 33.9 \pm 1.3$ kcal/mol is in good accord with the experimental result of the present study. The theoretical values $\Delta_f H°_0(C_6H_5) = 87.6 \pm 1.0$ kcal/mol and $\Delta_f H°_0(C_6H_5CO) = 33.9 \pm 1.3$ kcal/mol indicate the literature $\Delta_f H°_0$ values for C_6H_5CO and C_6H_5 are likely to be low by 3–4 kcal/mol.

[1] S. W. North, D. A. Blank, J. D. Gezelter, C. A. Longfellow, and Y. T. Lee, J. Chem. Phys. **102**, 4447 (1995).
[2] S. K. Kim, S. Pederson, and A. H. Zewail, J. Chem. Phys. **103**, 477 (1995).
[3] K. A. Trentelman, S. H. Kable, D. B. Moss, and P. L. Houston, J. Chem. Phys. **91**, 7498 (1989).
[4] P. D. Lightfoot, S. P. Kirwan, and M. J. Pilling, J. Phys. Chem. **92**, 4938 (1988).
[5] H. Li, Q. Li, W. Mao, Q. Zhu, and F. Kong, J. Chem. Phys. **106**, 5943 (1997).
[6] P. W. Kash, G. C. G. Waschewsky, R. E. Morss, and L. J. Butler, J. Chem. Phys. **100**, 3463 (1994).
[7] S. W. North, D. A. Blank, and Y. T. Lee, Chem. Phys. Lett. **224**, 38 (1994).
[8] S. Deshmukh and W. P. Hess, J. Chem. Phys. **100**, 6429 (1994).
[9] S. Deshmukh, J. D. Myers, S. S. Xantheas, and W. P. Hess, J. Phys. Chem. **98**, 12535 (1994).
[10] J. G. Calvert and J. N. Pitts, *Photochemistry* (Wiley, New York, 1966).
[11] N. C. Baird and H. B. Kathpal, Can. J. Chem. Phys. **55**, 863 (1977).
[12] W. C. Brider, *Combustion Chemistry* (Springer, New York, 1984).
[13] H. H. Glazebrook and T. G. Pearson, J. Chem. Soc. **589** (1939).
[14] F. J. Duncan and A. F. Trotman-Dickenson, J. Chem. Soc. **1962**, 4672.
[15] M. Berger and C. Steel, J. Am. Chem. Soc. **97**, 4817 (1975).
[16] L. A. Curtiss, K. Raghavachari, G. W. Trucks, and J. A. Pople, J. Chem. Phys. **94**, 7221 (1991).
[17] L. A. Curtiss, K. Raghavachari, and J. A. Pople, J. Chem. Phys. **98**, 1293 (1993).
[18] B. J. Smith and L. Radom, J. Phys. Chem. **99**, 6468 (1995).
[19] Y. S. Cheung, Y.-J. Chen, C.-L. Liao, C. Y. Ng, and W.-K. Li, J. Am. Chem. Soc. **117**, 9725 (1995).
[20] C. W. Bauschlicher, Jr., J. Phys. Chem. **98**, 2564 (1994).
[21] S. G. Lias, J. E. Bartmess, J. F. Liebman, J. L. Holmes, R. D. Levin, and W. G. Mallard, J. Phys. Chem. Ref. Data **17**, S 1 (1988).
[22] J. T. Niiranen, D. Gutman, and L. N. Krasnoperov, J. Phys. Chem. **96**, 5881 (1992).
[23] R. K. Solly and S. W. Benson, J. Am. Chem. Soc. **93**, 1592 (1971).
[24] S. W. Benson, *Thermochemical Kinetics* (Wiley, New York, 1968).
[25] W.-B. Tzeng, H.-M. Yin, W.-Y. Leung, J.-Y. Luo, S. Nourbakhsh, G. D. Flesch, and C. Y. Ng, J. Chem. Phys. **88**, 1658 (1988).
[26] H.-Q. Zhao, Y.-S. Cheung, C.-X. Liao, C. Y. Ng, W.-K. Li, and S.-W. Chiu, J. Chem. Phys. **104**, 130 (1996).
[27] H.-Q. Zhao, Y.-S. Cheung D. P. Heck, C. Y. Ng, T. Tetzlaff, and W. S. Jenks, J. Chem. Phys. **106**, 86 (1997).
[28] C. Y. Ng, Adv. Photochem. **22**, 1 (1997).
[29] T. K. Minton, G. M. Nathanson, and Y. T. Lee, J. Chem. Phys. **86**, 1991 (1987).
[30] E. J. Hintsa, X. Zhao, and Y. T. Lee, J. Chem. Phys. **92**, 2280 (1990).
[31] X. Zhao, Ph.D. thesis, University of California, Berkeley, CA (1988).
[32] S.-W. Chiu, W.-K. Li, W.-B. Tzeng, and C. Y. Ng, J. Chem. Phys. **97**, 6557 (1992).
[33] M. J. Frisch *et al.*, GAUSSIAN 94 (Gaussian, Pittsburgh, PA, 1994).
[34] A. Nicolades and L. Random, Mol. Phys. **88**, 759 (1996).
[35] L. A. Curtiss, K. Raghavachari, P. C. Redfern, and J. A. Pople, J. Chem. Phys. **106**, 1063 (1997).
[36] G. E. Davico, V. M. Bierbaum, C. H. DePuy, G. B. Ellison, and R. R. Squires, J. Am. Chem. Soc. **117**, 2590 (1995).
[37] M. N. Glukhovtsev and S. Laiter, Theor. Chim. Acta **92**, 32 (1995).
[38] K. Raghavachar, B. B. Stefanov, and L. A. Curtiss, J. Chem. Phys. **106**, 6764 (1997).
[39] The portion of the true $P(E_{c.m.})$ at $E_{c.m.} < 10.5$ kca/mol for process (2) is higher than that shown by the approximated $P(E_{c.m.})$. Thus, the true $P(E_{c.m.})$ is expected to peak at a $E_{c.m.}$ lower than 10.5 kcal/mol.
[40] R. N. Zare, Mol. Photochem. **4**, 1 (1972).
[41] J. G. Frey and P. Felder, Mol. Phys. **75**, 1419 (1992).